Nuclear Instruments and Methods in Physics Research B 505 (2021) 24–33

Contents lists available at ScienceDirect

Nuclear Inst. and Methods in Physics Research, B

journal homepage: www.elsevier.com/locate/nimb

Cross section measurement of alpha-particle-induced reactions on ^{nat}Sb

S. Takács [a,*], F. Ditrói [a], Z. Szűcs [a], K. Brezovcsik [a], H. Haba [b], Y. Komori [b], M. Aikawa [c,d], M. Saito [d], T. Murata [d], M. Sakaguchi [d], N. Ukon [e]

[a] Institute for Nuclear Research, (ATOMKI), 4026 Debrecen, Hungary
[b] Nishina Center for Accelerator-Based Science, RIKEN, Wako 351-0198, Japan
[c] Faculty of Science, Hokkaido University, Sapporo 060-0810, Japan
[d] Graduate School of Biomedical Science and Engineering, Hokkaido University, Sapporo 060-8638, Japan
[e] Advanced Clinical Research Center, Fukushima Medical University, Fukushima 960-1295, Japan

ARTICLE INFO

Keywords:
^{nat}Sb target
Alpha-particle-induced reaction
Stack-foil activation
Off-line γ-ray spectrometry
Excitation function

ABSTRACT

Cross sections of alpha-particle induced reactions were determined on antimony targets using alpha-particle irradiation with a primary energy of 50 MeV. The standard stacked target technique, activation method and offline gamma-ray spectrometry were applied for determination of the reaction cross sections. Thin Sb targets prepared by vacuum evaporation onto Kapton backings were activated. Ti foils were inserted into the stack for monitoring the alpha-particle beam parameters and energy loss of the particles in the target by using the ^{nat}Ti(α, x)^{51}Cr monitor reaction. Reaction cross sections for formation of ^{121,123,124,125,126}I, ^{121m,g,123m,125m}Te and ^{118m,120m,122g}Sb were determined and compared to the available literature data and theoretical estimation of the cross sections from the TENDL-2019 data library.

1. Introduction

The aim of this work was to investigate in general the excitation functions of alpha-particle-induced nuclear reactions on antimony targets. Thin Sb targets with natural isotopic composition, prepared by vacuum evaporation onto Kapton (polyimide) backings were irradiated and activated with a 50.42-MeV alpha-particle beam to deduce the experimental cross section data. The standard stacked-foil technique, the activation method, and the off-line gamma-ray spectrometry were applied to determine elemental activation cross section data for the reactions induced in the Sb targets by the alpha-particle beam. Excitation functions were constructed from their respective threshold energy up to 50 MeV. Due to technical limitations, formation of isotopes with half-lives between 1 h and 1 year were investigated. Hence, the reactions $^{nat}Sb(\alpha,x)^{121}I$, $^{nat}Sb(\alpha,x)^{123}I$, $^{nat}Sb(\alpha,x)^{124}I$, $^{nat}Sb(\alpha,x)^{125}I$ and $^{nat}Sb(\alpha,x)^{126}I$ for formation of iodine isotopes were studied. These radioisotopes can be interesting for medical applications as the main or side products. Formation of Te isotopes in the $^{nat}Sb(\alpha,x)^{121m,g}Te$, $^{nat}Sb(\alpha,x)^{123m}Te$ and $^{nat}Sb(\alpha,x)^{125m}Te$ reactions and Sb isotopes in the $^{nat}Sb(\alpha,x)^{118m}Sb$, $^{nat}Sb(\alpha,x)^{120m}Sb$, and $^{nat}Sb(\alpha,x)^{122g}Sb$ reactions were also observed. The measured cross section data were compared to the available experimental data measured earlier. The newly measured cross sections were also compared to the results of the TALYS theoretical model code calculation taken from the TENDL-2019 data library. The widely used TENDL data library contains data calculated by using default input parameters. Comparing the tabulated theoretical results with the experimental data may contribute to the development of the TALYS model code and could result in an improved predicting capability.

2. Experimental

The experiment was performed at the AVF cyclotron laboratory of Nishina Center for Accelerator-Based Science, RIKEN, Japan. For activation of the Sb targets, the standard activation method using the stacked-foil target technique was applied followed by high resolution off-line gamma-ray spectrometry for determining the radioactivity of the reaction products in each irradiated foil.

The Sb targets were prepared by depositing an antimony layer using vacuum evaporation onto Kapton backing (nominal thickness 25 μm, Goodfellow, Co., Ltd., UK). The Kapton backings of 13 mm in diameter were cut and measured by weight before Sb evaporation using a Mettler Toledo XPR2U digital microbalance (d = 0.1 μg). As the melting point of Sb is relatively low (T_m = 636.6C), it is easy to prepare thin Sb targets by using the vacuum evaporation method [1]. Small grains of Sb (about 5

* Corresponding author.
E-mail address: stakacs@atomki.hu (S. Takács).

https://doi.org/10.1016/j.nimb.2021.08.008
Received 30 June 2021; Received in revised form 17 August 2021; Accepted 24 August 2021
Available online 1 September 2021
0168-583X/© 2021 The Author(s). Published by Elsevier B.V. This is an open access article under the CC BY-NC-ND license (http://creativecommons.org/licenses/by-nc-nd/4.0/).

mg) were placed in a Ta boat to heat it up under vacuum and create Sb vapor, which was deposited as a thin layer of antimony onto the Kapton backing. The Kapton backings with masks of 10 mm in diameter in front were placed about 15 cm from the source of evaporating Sb. This geometry provided relatively even Sb layers on the Kapton backings. Seven Sb target foils were prepared in one evaporation run. After evaporation each Kapton foil was weighted again and the thickness of the evaporated Sb layer was determined. Due to statistical behavior of the evaporation process the thickness of each created Sb layer was different. The evaporated Sb targets were ordered by weight and the foils with the lightest and the heaviest weight of Sb layers were paired. The selected foils of each pair were placed Sb face-to-face enclosing the Sb layers between the two Kapton backings. Thus 25 Kapton-Sb-Kapton sandwich targets were created, from which 22 were used in the experiment. The average thickness of the Sb layer in the sandwich target was about 1.5 μm (~1 mg/cm^2). Additional Ti-Kapton foil pairs were inserted into the stack for beam monitoring purposes. To monitor the beam parameters the cross sections of the $^{nat}Ti(\alpha,x)^{51}Cr$ reaction were determined for every Ti foil, and were compared with the recommended values provided by IAEA [2]. The additional Kapton foils behind the Ti foils served to catch the reaction recoiled products. Both the Ti and Kapton foils were cut from a larger sheet, of which the surface area and the weight were measured beforehand and an average thickness was determined for both materials. The thickness of the Ti foils was 5.3 ± 0.05 μm (99.9%, Nilaco Corp., Japan), while the average thickness of the Kapton foil was 24.5 ± 0.25 μm. These average thicknesses were used in the data analysis.

The energy of the alpha particle beam was set by the basic parameters of the cyclotron. After fine tuning of the cyclotron and passing the alpha-particle beam through the beam transport system the energy was measured by the time-of-flight method using electrostatic pickups [3]

Table 1
Reaction and decay data used in the data analysis taken from NuDat2 [5], LiveChart [7] and QCalc [6].

Radio-nuclide	Half-life	Gamma energy (keV)	Gamma-intensity (%)	Contributing reactions	Q-value (MeV)	Threshold (MeV)
^{51}Cr	27.704 d	320.0824	9.910 *10*	^{48}Ti(α,n)^{51}Cr	−2.69	2.91
				^{49}Ti(α,2n)^{51}Cr	−10.83	11.72
				^{50}Ti(α,3n)^{51}Cr	−21.77	23.51
^{121}I	2.12 h	212.2	84.3 *3*	^{121}Sb(α,4n)^{121}I	−30.50	31.50
				^{123}Sb(α,6n)^{121}I	−48.98	50.57
^{123}I	13.2234 h	158.97	83.3 *4*	^{121}Sb(α,2n)^{123}I	−15.37	15.88
				^{123}Sn(α,4n)^{123}I	−31.12	32.16
^{124}I	4.1760 d	1509.36	3.25 *5*	^{121}Sb(α,n)^{124}I	−7.88	8.14
				^{123}Sn(α,3n)^{124}I	–23.65	24.42
^{125}I	59.400 d	35.4925	6.68 *13*	^{121}Sb(α,γ)^{125}I	1.66	0.0
				^{123}Sb(α,2n)^{125}I	−14.10	14.56
^{126}I	12.93 d	388.633	35.6 *6*	^{123}Sb(α,n)^{126}I	−6.96	7.19
		666.331	32.9 *7*			
^{121g}Te	19.17 d	573.139	80.4 *22*	^{121}Sb(α,nt)^{121}Te	−21.65	22.37
				^{121}Sb(α,2nd)^{121}Te	−27.91	28.83
				^{121}Sb(α,3np)^{121}Te	−30.13	31.13
^{121m}Te	164.2 d	212.189	81.5 *10*	^{121}Sb(α,nt)^{121}Te	−21.94	22.66
				^{121}Sb(α,2nd)^{121}Te	−28.20	29.12
				^{121}Sb(α,3np)^{121}Te	−30.42	31.42
^{123m}Te	119.2 d	159.00	84.0 *4*	^{121}Sb(α,d)^{123m}Te	−11.39	11.76
				^{121}Sb(α,np)^{123m}Te	−13.61	14.05
				^{123}Sb(α,nt)^{123m}Te	−20.90	21.57
				^{123}Sb(α,2nd)^{123m}Te	−27.15	28.03
				^{123}Sb(α,3np)^{123m}Te	−29.38	30.33
^{125m}Te	57.40 d	35.504	7.30 *7*	^{123}Sb(α,d)^{125}Te	−10.91	11.27
				^{123}Sb(α,np)^{125}Te	−13.14	13.56
^{118m}Sb	5.00 h	1050.69	97 *5*	^{121}Sb(α,3nα)^{118m}Sb	−25.82	26.67
		1229.65	100 *5*	^{121}Sb(α,n2t)^{118m}Sb	−37.15	38.38
				^{121}Sb(α,2ndt)^{118m}Sb	−43.41	44.84
				^{121}Sb(α,npt)^{118m}Sb	−45.63	47.14
				^{121}Sb(α,4n^{3}He)^{118m}Sb	−46.40	47.93
				^{123}Sb(α,5nα)^{118m}Sb	−41.58	42.94
^{120m}Sb	5.76 d	197.3	87.0 *11*	^{121}Sb(α,nα)^{120m}Sb	−9.254	9.56
		1023.3	99.4 *3*	^{121}Sb(α,dt)^{120m}Sb	−26.84	27.73
		1171.7	100 *0*	^{121}Sb(α,npt)^{120m}Sb	−29.07	30.03
				^{121}Sb(a,2n^{3}He)^{120m}Sb	−29.83	30.82
				^{121}Sb(α,n2d)^{120m}Sb	–33.1	34.20
				^{121}Sb(α,2npd)^{120m}Sb	−35.32	36.49
				^{121}Sb(α,3n2p)^{120m}Sb	−37.55	38.79
				^{123}Sb(α,3na)^{120m}Sb	−25.02	25.83
				^{123}Sb(α,n2t)^{120m}Sb	−36.35	37.54
				^{123}Sb(α,2ndt)^{120m}Sb	−42.61	44.00
				^{123}Sb(α,3npt)^{120m}Sb	−44.83	46.29
				^{123}Sb(α,4n^{3}He)^{120m}Sb	−45.598	47.083
				^{123}Sb(α,3n2d)^{120m}Sb	−48.867	50.458
^{122g}Sb	2.7238 d	564.24	70.68 *18*	^{121}Sb(α,^{3}He)^{122g}Sb	−13.77	14.23
				^{121}Sb(α,dp)^{122g}Sb	−19.26	19.90
				^{121}Sb(α,n2p)^{122g}Sb	−21.6	22.20
				^{123}Sb(α,nα)^{122g}Sb	−8.96	9.252
				^{123}Sb(α,dt)^{122g}Sb	−26.55	27.41
				^{123}Sb(α,npt)^{122g}Sb	−28.77	29.71
				^{123}Sb(α,2n^{3}He)^{122g}Sb	−29.54	30.5
				^{123}Sb(α,n2d)^{122g}Sb	–32.81	33.87
				^{123}Sb(α,2npd)^{122g}Sb	−35.03	36.17
				^{123}Sb(α,3n2p)^{122g}Sb	−37.26	38.46

before and after the irradiation. The initial energy of the used alpha-particle beam was 50.42 ± 0.2 MeV. The beam intensity was kept constant during the 2 h irradiation and was about 50nA (25 particle nA). The intensity of the beam was recorded every 30 s to follow its stability. No correction was necessary to apply for beam fluctuation. The design of the Faraday cup type target holder assured minimal loss of secondary electrons even without applying a suppression voltage due to its low solid angle opening in backwards direction. The primary beam intensity measured by charge collection on the target was corrected in accordance with the $^{nat}Ti(\alpha,x)^{51}Cr$ monitor reaction. No correction was applied for the primary measured beam energy. The energy degradation of the beam through the layered target was estimated by calculation using the polynomial approximation of the stopping power by Andersen and Ziegler [4]. No correction was necessary to apply for the energy loss of the alpha-particles passing through the target.

To record the gamma-ray spectra of the activated foils a high-resolution off-line gamma-spectrometer was used, consisted of a HPGe detector (ORTEC GEM-25185-P), ORTEC nuclear electronics, and the SEIKO EG&G Gamma Studio acquisition and analyzing software. The detector was calibrated for the energy- and geometry-dependent efficiencies on a usual way, by using a standard multiple γ-ray point source consisting of ^{57,60}Co, ^{88}Y, ^{109}Cd, ^{113}Sn ^{137}Cs, ^{139}Ce and ^{241}Am radioisotopes. The spectra of the activated foils were recorded several times without chemical separation to assess the activity of each produced radionuclide with different half-lives. Three series of spectra were recorded with average cooling times of 25, 75, and 180 h. The reaction- and decay-parameters used in the data analysis were taken from the NuDat2.8 [5], QCalc [6], and LiveChart [7] data libraries and are summarized in Table 1.

Cross sections for the investigated reactions were deduced using Eq. 1., based on the well-known activation and decay lows and used in several of our earlier publications [8–20].

$$\sigma = \frac{T_\gamma \lambda}{\varepsilon_d \varepsilon_\gamma N_t N_b (1 - e^{-\lambda t_b}) e^{-\lambda t_c} (1 - e^{-\lambda t_m})} \quad (1)$$

The cross section in each target foil was calculated from the primary experimental data according to the above equation: surface density of target atoms N_t [1/cm^2], number of bombarding particles per unit time N_b [1/s], number of counts in the photo-peak T_γ, detector efficiency ε_d, gamma ray abundance ε_γ, measurement dead time ε_t, decay constant λ [1/s], bombarding time t_b [s], cooling time t_c [s] and acquisition time t_m [s]. Using the well-known activation and decay laws elemental cross sections were deduced based on the recorded spectra. The elemental cross section is a linear combination of the cross sections determined for the nuclear reactions occurred on the different stable isotopes of the target with natural isotopic abundance, resulted the same radionuclide. The weighting factors in the linear combination are the natural abundance of the target isotopes. The cross section in this work is considered to be independent or direct when no decay contribution is available to the formation of the investigated radionuclide. Accordingly, a cross section is considered to be cumulative when besides the direct process decay-production also contributes to the formation of the radionuclide. The uncertainty associated with the deduced cross sections was estimated as the square root of the quadratic summation of each relative uncertainty component. The linearly propagating partial uncertainties were considered to contribute to the total uncertainty. These are: number of target atoms 1.0%, beam intensity including correction 5.9%, decay gamma-ray intensities 0.3–25.47%, detector efficiency 4–6%, statistical uncertainty including peak fitting uncertainty 0.6–39%. Uncertainty of time parameters was not included due to the relatively long half-lives of the investigated isotopes. The uncertainty of the primary beam energy provided by the used TOF method was ±0.2 MeV. The uncertainty of the mean energy of the alpha-particles for each foil in the stack was estimated considering the uncertainty of the primary beam energy and the uncertainty of the foil thicknesses. An upper limit and a lower limit of the energy loss were calculated for every layer in the stack, then the deviations from the corresponding mean energy were determined. Due to the straggling effect the initial energy distribution of the alpha-particle beam widened, which in addition increased the overall uncertainty of the calculated mean energy for every foil [21]. The estimated total uncertainty of the mean energy reached ±1.44 MeV for the last Sb layer in the stack.

The numerical values of the deduced experimental cross sections are presented in Tables 2–4. Data are also presented graphically in Figs. 2–13 in comparison with the experimental data measured earlier if those were available and the result of an independent TALYS model calculation taken from the TENDL-2019 data library [22]. Cross section data measured on enriched target isotopes were converted to correspond to natural Sb target. The numerical data of the earlier experimental works were retrieved from the IAEA EXFOR database [23].

3. Results and discussion

3.1. The $^{nat}Ti(\alpha,x)^{51}Cr$ monitor reaction

From the activated Ti foils energy dependent cross sections were calculated for the $^{nat}Ti(\alpha,x)^{51}Cr$ monitor reaction using the $E_\gamma = 320$ keV ($I_\gamma = 9.91\%$) gamma-line. The recoil correction was not necessary to apply for the activity measurement of the Ti foils, since each Ti foil was measured together with its following Kapton catcher foil. The deduced cross sections were compared with the recommended values provided by the International Atomic Energy Agency [2]. The primary beam intensity measured experimentally was corrected by 3.5% to compensate the small difference between the recommended and the experimentally measured values. The adapted beam intensity of 52.2 ± 3.1nA provided a good agreement for the amplitude between the measured and recommended values, and was used in data analysis. The energy, associated with the deduced cross sections, calculated from the energy loss of the alpha-particles in the stack provided also a very good agreement with the recommended values.

3.2. Production of iodine radionuclides

Iodine isotopes are produced in the (α,xn) reactions on the two stable isotopes of antimony. Considering bombardment of Sb target with an alpha-particle beam of 50 MeV formations of iodine isotopes is energetically possible in the mass region between 120 and 127. Among these possible iodine isotopes, the ^{127}I is stable, and the iodine isotopes ^{120,122}I have too short half-lives to be able to detect them in our experimental conditions. Thus, in this work cross sections were deduced only for formation of the ^{121,123,124,125,126}I radionuclides.

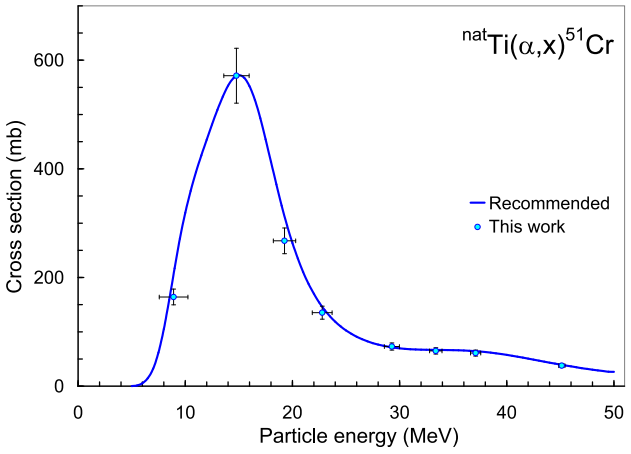

Fig. 1. Experimental cross sections of the $^{nat}Ti(\alpha,x)^{51}Cr$ monitor reaction after corrections in comparison with the recommended values.

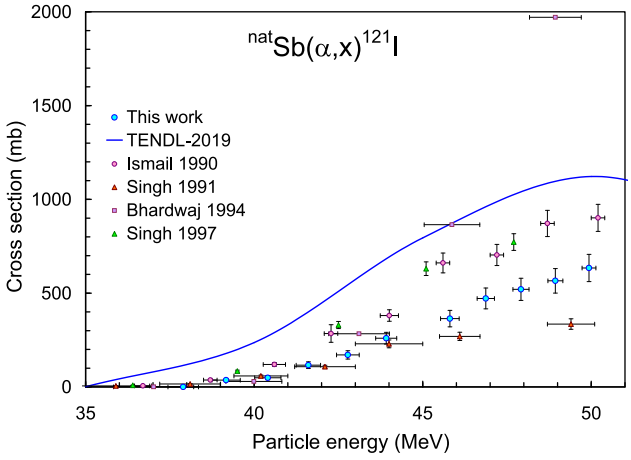

Fig. 2. Experimental cross sections of the $^{nat}Sb(\alpha,x)^{121}I$ reaction in comparison with the earlier reported data sets and the result of theoretical calculation.

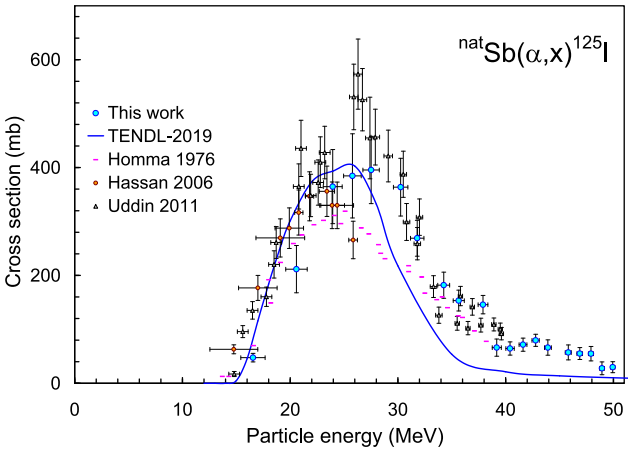

Fig. 5. Experimental cross sections of the $^{nat}Sb(\alpha,x)^{125}I$ reaction in comparison with the earlier reported data sets and result of theoretical calculation.

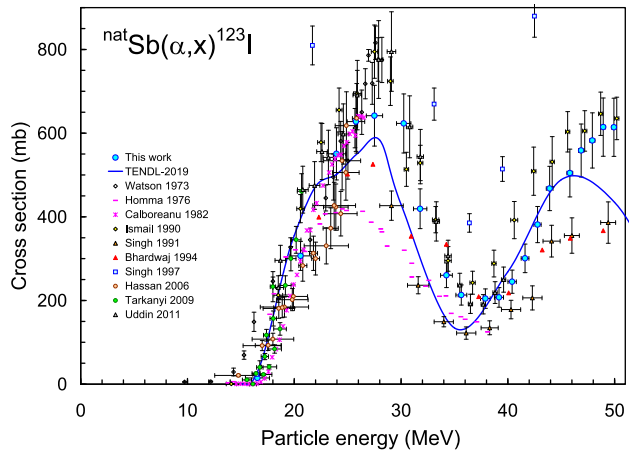

Fig. 3. Experimental cross sections of the $^{nat}Sb(\alpha,x)^{123}I$ reaction in comparison with the earlier reported data sets and result of theoretical calculation.

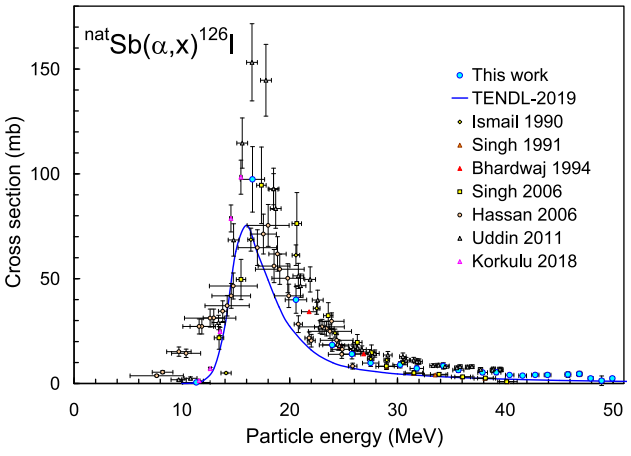

Fig. 6. Experimental cross sections of the $^{nat}Sb(\alpha,x)^{126}I$ reaction in comparison with the earlier reported data sets and result of theoretical calculation.

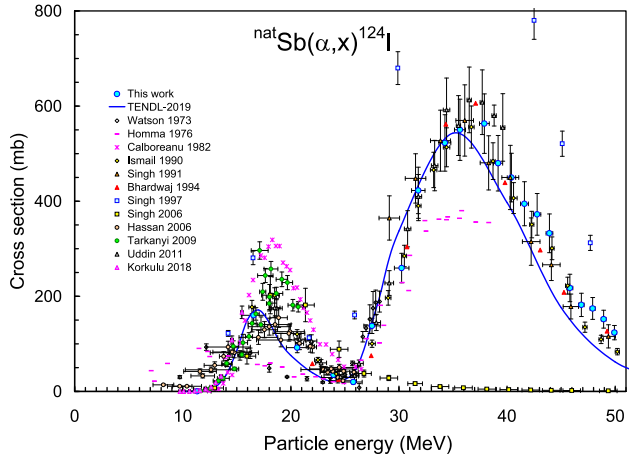

Fig. 4. Experimental cross sections of the $^{nat}Sb(\alpha,x)^{124}I$ reaction in comparison with the earlier reported data sets and result of theoretical calculation.

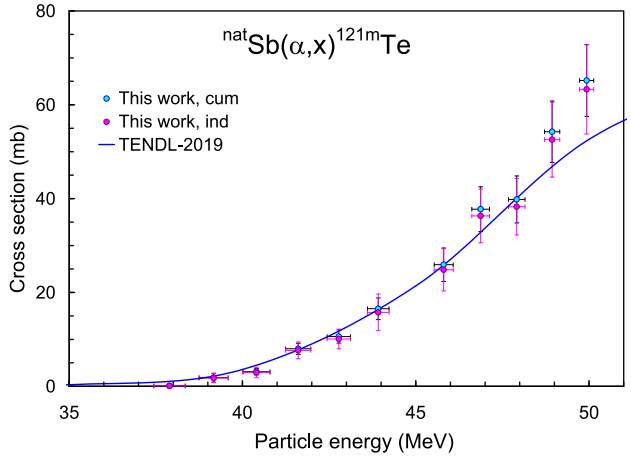

Fig. 7. Cumulative and independent experimental cross sections of the $^{nat}Sb(\alpha,x)^{121m}Te$ reaction in comparison with the result of theoretical calculation (TENDL-2019 [22]).

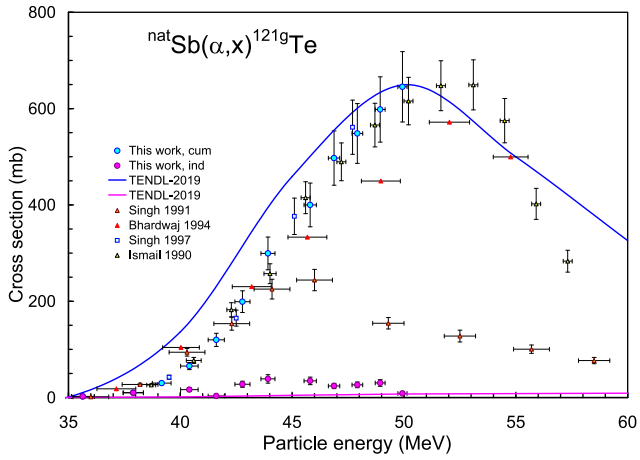

Fig. 8. Cumulative and independent experimental cross sections of the $^{nat}Sb(\alpha,x)^{121g}Te$ reaction in comparison with the available literature data and result of theoretical calculation (TENDL-2019 [22]).

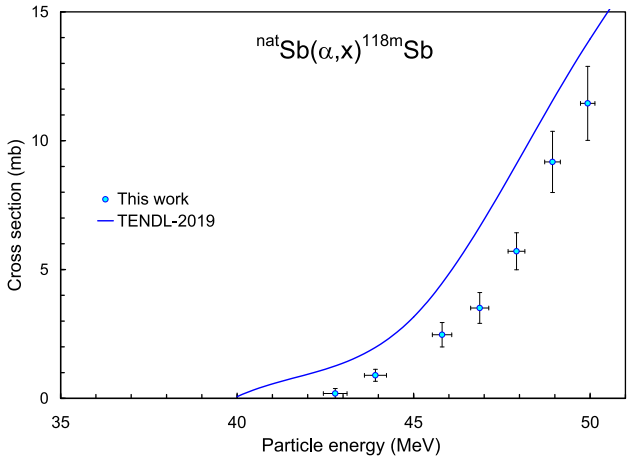

Fig. 11. Experimental cross sections of the $^{nat}Sb(\alpha,x)^{118m}Sb$ reaction in comparison with the result of TALYS theoretical model calculation (TENDL-2019 [22]).

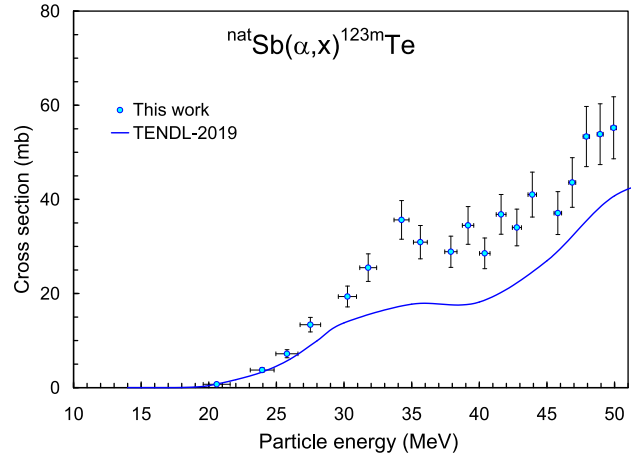

Fig. 9. Experimental cross sections of the $^{nat}Sb(\alpha,x)^{123m}Te$ reaction in comparison with the result of TALYS theoretical model calculation (TENDL-2019 [22]).

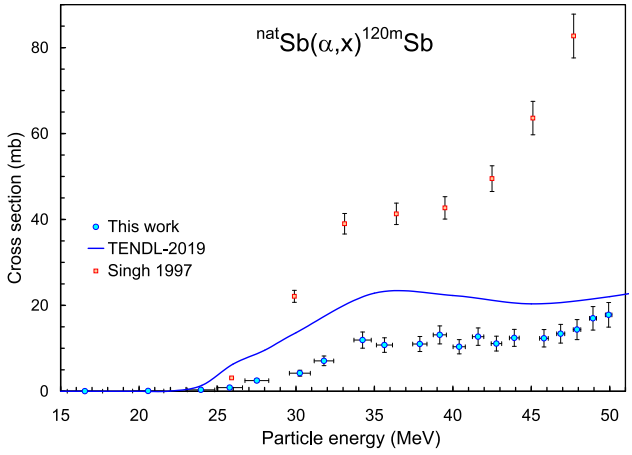

Fig. 12. Experimental cross sections of the $^{nat}Sb(\alpha,x)^{120m}Sb$ reaction in comparison with the earlier reported data [27] and result of the TALYS theoretical model calculation (TENDL-2019 [22]).

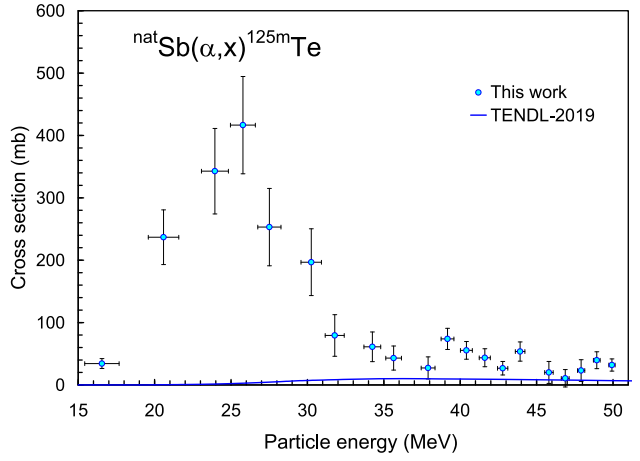

Fig. 10. Experimental cross sections of the $^{nat}Sb(\alpha,x)^{125m}Te$ reaction in comparison with the result of TALYS theoretical model calculation (TENDL-2019 [22]).

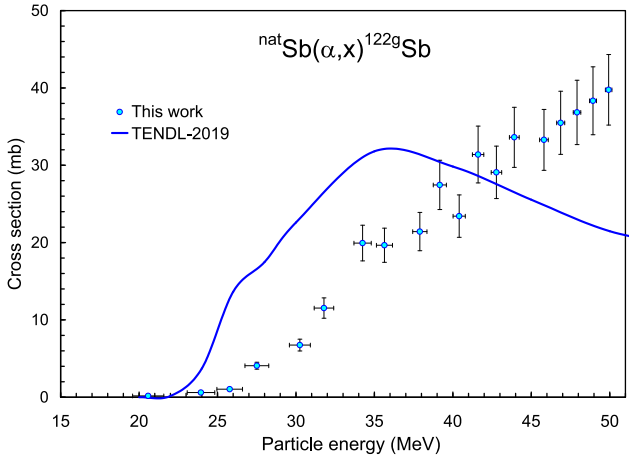

Fig. 13. Experimental cross sections of the $^{nat}Sb(\alpha,x)^{122g}Sb$ reaction in comparison with the result of TALYS theoretical model calculation (TENDL-2019 [22]).

3.2.1. Experimental cross sections of the $^{nat}Sb(\alpha,x)^{121}I$ process

The radionuclide ^{121}I can be formed in the $^{121}Sb(\alpha,4n)^{121}I$ and $^{123}Sb(\alpha,6n)^{121}I$ reactions. But contribution from the $^{123}Sb(\alpha,6n)^{121}I$ reaction can be neglected in this experiment, since the threshold energy of the reaction is 50.57 MeV. Even though, only the $^{121}Sb(\alpha,4n)^{121}I$ reaction is considered the measured data were not normalized by the isotopic abundance of ^{121}Sb, hence the presented cross section data correspond to the natural antimony target. The ^{121}I has a half-life $T_{1/2} = 2.12$ h. It decays almost 100% to the ground state of ^{121}Te. In the data analysis the $E_\gamma = 212$ keV, the only strong gamma-line of ^{121}I, was used. Due to the long half-life of ^{121m}Te correction for contribution from decay of ^{121m}Te to the $E_\gamma = 212$ keV gamma line is straightforward. The cross sections of the $^{nat}Sb(\alpha,x)^{121}I$ reaction are presented in Fig. 2 in comparison with the earlier experimental data and the result of TALYS theoretical calculation taken from the TENDL-2019 database [22]. Numerical data are collected in Table 2. There are four data sets reported earlier [24,25,26,27]. They are more or less in agreement with our data up to 40 MeV. Above the practical threshold energy of the $^{nat}Sb(\alpha,x)^{121}Te$ reaction, (~40 MeV) data of Singh 1991 [25] are too low and data of Bhardwaj 1994 [26] are extremely too high (out of scale), which may originate from inappropriate evaluation of the contribution from the decay of ^{121m}Te. The TALYS calculation gives an over estimation of the experimental data in the whole energy region.

3.2.2. Experimental cross sections of the $^{nat}Sb(\alpha,x)^{123}I$ process

Reactions on both ^{121}Sb and ^{123}Sb isotopes can contribute to the formation of ^{123}I radionuclide. In the data analysis $T_{1/2} = 13.2234$ h half-life and $E_\gamma = 158.97$ keV ($I_\gamma = 83.3\%$) were used. The only intense gamma-line that follows the decay of ^{123}I is the $E_\gamma = 158.97$ keV gamma-ray, which is disturbed by the same energy gamma-line from decay of the longer-lived ^{123m}Te and the shorter-lived ^{117}Sb. Due to the applied waiting time, contribution to the peak area from decay of ^{117}Sb was avoided. Contributions to the measured peak area of the $E_\gamma = 158.97$ keV gamma-line from the two decaying radionuclides, ^{123}I and ^{123m}Te, can be determined and separated based on their much different half-lives. By applying long decay times the activity of ^{123}I can be reduced and its contribution to the peak area of the $E_\gamma = 158.97$ keV gamma-line is at a negligible level and the cross section for formation of ^{123m}Te can be determined. Knowing the cross section of the $^{nat}Sb(\alpha,x)^{123m}Te$ process its contribution to the peak area in a spectra measured after a shorter decay time, can be calculated and subtracted and the cross section of the direct formation of ^{123}I can be determined. To determine the cross section for formation of ^{123m}Te the spectra collected after an average decay time of 180 h were used, while for determining the cross sections for formation of ^{123}I the first series of spectra with an average decay time of about 25 h were used. The deduced cross section data for the $^{nat}Sb(\alpha,x)^{123}I$ process are collected in Table 2 and presented in Fig. 3 in comparison with the earlier experimental data and the result of the TALYS theoretical calculation taken from the TENDL-2019 database [22]. The contribution of the two reactions $^{121}Sb(\alpha,2n)^{123}I$ and $^{123}Sb(\alpha,4n)^{123}I$ clearly can be identified. Both, the experimental data and the result of the theoretical calculation reveal double peak excitation function according to the two reactions. There are ten earlier reported data sets [24,25,26,27,28,29,30,31,32,33]. Data measured on enriched antimony target isotopes were converted to Sb target with natural isotopic composition. All data series follow the average shape of the excitation function, but they exhibit large differences in amplitude.

Data of Singh et al. 1997 [27] are improperly too high. They are a factor of two higher than the average of the other reported data. For most of the literature data it is difficult to identify if they have an energy shift or amplitude problem. Most data were measured by using the stacked target technique, which may easily introduce large energy uncertainty at the low energy part of the target stack. Calboreanu et al. [30] used single target irradiation technique combined with time-of-flight, TOF, energy measurement; therefore their data may represent the proper energy scale. This is confirmed by the energy scale of our data, which was compared to the monitor reaction $^{nat}Ti(\alpha,x)^{51}Cr$, see Fig. 1. Comparing the TENDL-2019 data to our experimental result an overall agreement can be found, except at the two local maxima of the excitation function, where the theoretical curve somewhat underestimates our results.

3.2.3. Experimental cross sections of the $^{nat}Sb(\alpha,x)^{124}I$ process

The ^{124}I radionuclide is formed in the $^{121}Sb(\alpha,n)^{124}I$ and $^{123}Sb(\alpha,3n)^{124}I$ reactions. It decays to ^{124}Te and the decay is followed by emission of several characteristic gamma-lines, most of them are in interference with the same energy gamma-lines from decay of the co-produced ^{124}Sb. The half-lives of these two radionuclides are different; therefore separation of their contribution to a common gamma-line in the gamma-spectra is possible. However, using the $E_\gamma = 1509.36$ keV ($I_\gamma = 3.25\%$) relatively weak but interference free gamma-line, such separation process can be avoided. For data analysis the second series of

Table 2
Cross sections for formation of iodine radioisotopes on ^{nat}Sb target by alpha-particle irradiation.

Energy (MeV)			Cross section (mb)															
			$^{nat}Sb(\alpha,x)^{121}I$			$^{nat}Sb(\alpha,x)^{123}I$			$^{nat}Sb(\alpha,x)^{124}I$			$^{nat}Sb(\alpha,x)^{125}I$			$^{nat}Sb(\alpha,x)^{126}I$		
49.93	±	0.21	634	±	73	614	±	70	124	±	15	29.8	±	10.2	2.4	±	0.9
48.94	±	0.22	566	±	65	614	±	70	152	±	19	27.7	±	11.9	1.3	±	2.3
47.92	±	0.24	520	±	59	582	±	66	175	±	23	54.9	±	13.4	2.4	±	0.9
46.87	±	0.26	472	±	56	559	±	63	182	±	24	55.1	±	11.1	4.6	±	1.3
45.81	±	0.28	364	±	44	505	±	57	218	±	29	57.2	±	13.9	4.3	±	1.3
43.92	±	0.31	260	±	31	468	±	53	332	±	41	66.2	±	14.3	4.1	±	0.9
42.78	±	0.34	171	±	22	381	±	43	372	±	44	79.6	±	11.2	4.1	±	0.8
41.61	±	0.36	116	±	18	301	±	34	395	±	46	71.6	±	12.1	3.7	±	0.7
40.40	±	0.39	49	±	11	245	±	28	450	±	51	64.5	±	12.3	4.0	±	0.7
39.17	±	0.42	36	±	6	207	±	23	480	±	58	66.1	±	16.0	5.3	±	1.1
37.90	±	0.45	0.12	±	0.4	205	±	23	563	±	62	146	±	17	5.2	±	1.0
35.64	±	0.51				213	±	24	550	±	64	153	±	19	6.4	±	1.1
34.25	±	0.55				260	±	29	522	±	59	182	±	24	8.4	±	1.5
31.79	±	0.62				419	±	47	423	±	49	269	±	33	7.2	±	1.2
30.25	±	0.67				623	±	71	259	±	31	364	±	54	8.9	±	1.5
27.51	±	0.76				642	±	73	138	±	16	396	±	62	9.8	±	1.6
25.78	±	0.82				628	±	71	19.9	±	4.0	385	±	78	14.0	±	2.9
23.95	±	0.88				551	±	62	34.9	±	4.2	365	±	69	18.4	±	3.0
20.58	±	1.00				307	±	35	92.2	±	10.8	212	±	44	39.9	±	6.4
16.55	±	1.13				14.9	±	1.7	160	±	18	47.5	±	8.0	97.4	±	15.6
11.34	±	1.27							0.44	±	0.13				0.5	±	0.1

gamma-spectra with an average decay time of about 75 h were used. The obtained cross section data are collected in Table 2 and presented in Fig. 4 in comparison with the available earlier experimental data and result of TALYS theoretical calculation taken from the TENDL-2019 database [22]. Cross section data measured on enriched Sb target material were converted to a target with the natural isotopic abundances. The excitation function has two local maxima which correspond to the two contributing reactions. The experimental data and the theoretical calculation follow the same shape and they show a reasonably good agreement.

There are twelve earlier reported experimental data sets [24–33,34,35]. Again, data of Singh et al. 1997 [27] are extremely too high. The data of Homma et al. 1976 [29] are too low. The rest of the data follow the main pattern of the excitation function, although their amplitudes are much different especially in the low energy segment. The TALYS code predicts the excitation function fairly well.

3.2.4. Experimental cross sections of the $^{nat}Sb(\alpha,x)^{125}I$ process

The ^{125}I radionuclide can be produced in the $^{121}Sb(\alpha,\gamma)^{125}I$ and the $^{123}Sb(\alpha,2n)^{125}I$ reactions. The cross section for alpha-capture reaction is very low, therefore the measured excitation function corresponds to the $^{123}Sb(\alpha,2n)^{125}I$ reaction. To keep the consistency of this paper the deduced data were not normalized to 100% abundance of the ^{123}Sb target isotope, instead the natural abundance was used during the data analysis. The ^{125}I radionuclide ($T_{1/2}$ = 59.4 d) decays to ^{125}Te which has a meta-stable state with a very similar half-life ($T_{1/2}$ = 57.4 d) and decays by IT (100%) decay mode to ^{125g}Te. Both decays are followed by emission of the E_γ = 35.5 keV gamma-line. Although, the evaporated Sb target layer was in average 1.5 μm thick, absorption correction was calculated [36] for every foil, which included the self-absorption of the Sb layer and the absorption of the covering Kapton layer. For a 1 μm-thick (0.668 mg/cm^2) Sb layer the self-absorption correction factor is 1.0092, while the absorption factor of the Kapton layer (3.479 mg/cm^2) is 1.0008. Separation of the contributions of ^{125}I and ^{125m}Te to the peak area was performed analytically, by solving the corresponding two unknown-parameters systems of equations based on the spectra collected in the second and third series of the gamma-ray measurements. Due to the statistical behavior of the radioactive decay process the deduced result may contain larger uncertainties. The cross sections of the $^{nat}Sb(\alpha,x)^{125}I$ reaction are collected in Table 2 and in Fig. 5 in comparison with the available literature data and data of TENDL-2019. Four data sets were found in the literature [29,31,33,35]. The data measured on enriched Sb targets were normalized to the natural isotopic abundances. Korkulu et al. 2018 [35] published the data only for the $^{121}Sb(\alpha,\gamma)^{125}I$ reaction, which are not included in the figure as they are in micro-barn scale.

Due to separation of the ^{125m}Te contribution the resulted data points are more scattered, which is probably valid for all experimental data sets. The TALYS model code predicts the shape of the excitation function with proper amplitude, although above the maximum of the curve its amplitude is below the experimental data.

3.2.5. Experimental cross sections of the $^{nat}Sb(\alpha,x)^{126}I$ process

Even though the radionuclide ^{126}I ($T_{1/2}$ = 12.93 d) can be produced only in the $^{123}Sb(\alpha,n)^{126}I$ reaction the deduced cross section data were not normalized to a 100% enrichment level of the target isotope: the natural abundance (42.79%) was kept. Accordingly, the literature data published for enriched ^{123}Sb target were converted to data for the natural isotopic ratio. Cross sections were determined using the spectra collected in the third series of the gamma-ray measurements. Both the E_γ = 388.6 keV (I_γ = 35.6%) and E_γ = 666.3 keV (I_γ = 32.9%) gamma-lines were used in the data analysis and the average of the two results, weighted by their uncertainties, were calculated. Our data are presented in Table 2 and in Fig. 6 together with the earlier published results and the result of the TALYS model code calculation taken from the TENDL-2019 database [22].

Seven earlier publications on the relevant data were found [24,25,26,27,31,33,35]. The cross sections determined for 100% ^{123}Sb target were converted to the natural isotopic abundance. As a general consequence of the stacked target technique, the energy of the low energy data points have large uncertainty except for data of Korkulu et al. 2018 [35]. Our data in combination with the data of Korkulu et al. 2018 [35] determine a smooth curve for the excitation function of this reaction. The TALYS model code predicts the shape of the excitation function but with a lower amplitude than the experimental data.

3.3. Production of tellurium radionuclides

Isotopes with mass number from 118 to 126 are possible to be formed considering the Q-values of the reactions producing tellurium. In the applied experimental conditions we could determine activation cross sections only for formation of the ^{121m,g,123m,125m}Te radionuclides. Although, formation of the ^{118,119}Te radionuclides are energetically possible, due to the low probability of the involving reactions, the collected information in the spectra were not statistically significant to provide data with acceptable uncertainty.

3.3.1. Experimental cross sections of the $^{nat}Sb(\alpha,x)^{121m,g}Te$ process

Due to the reaction threshold energies the radionuclide ^{121}Te can be formed only in the $^{121}Sb(\alpha,x)^{121}Te$ reactions. The emitted particles in this reaction are the combinations of a proton and three neutrons. The ^{121}Te radionuclide has two isomeric states, the ground state ($T_{1/2}$ = 19.17 d) and a longer-lived meta-stable state ($T_{1/2}$ = 164.2 d) with IT decay mode (88.6%) and EC and β^+ decay mode (11.4%). To be consequent on regarding the target isotopic composition, the deduced cross sections were not normalized to 100% isotopic abundance. The data analysis was based on the most intense gamma-lines. The cross sections for formation of ^{121m}Te were assessed through the E_γ = 212.189 keV (I_γ = 81.5%) gamma-line, using the gamma spectra measured after an average decay time of 180 h, when ^{121}I decayed completely, and the E_γ = 212.189 keV gamma line originates only from the decay of ^{121m}Te. The decay of ^{121}I populates the ^{121m}Te isomeric state less than 0.3% only [37], which contribution was calculated and was subtracted. Both, the cumulative and independent cross sections were determined for the formation of ^{121m}Te. The data are presented in Table 3 and in Fig. 7 together with the result of the TALYS model code calculation taken from the TENDL-2019 database [22]. The TALYS model code with default input parameters predicts the excitation function well. No earlier published experimental data were found for this reaction.

The cross sections for formation of the ground state, ^{121g}Te ($T_{1/2}$ = 19.17 d), were assessed by using the E_γ = 573.179 keV (I_γ = 80.4%) gamma-line. The decay of ^{121m}Te ($T_{1/2}$ = 164.2 d) and the decay of ^{121}I ($T_{1/2}$ = 2.12 h) populate the ^{121g}Te ground state. Contribution from decay of ^{121}Sn to the measured peak area is not expected as the decay of ^{121m,g}Sn does not followed emission of the E_γ = 573.179 keV gamma-line. Both, the cumulative and independent cross sections were determined. The gamma-ray spectra measured after an average decay time of 180 h were used in the data analysis. After this long decay time ^{121}I decayed completely, but the ^{121m}Te *meta*-stable state, with much longer half-life ($T_{1/2}$ = 164.2 d) and IT decay mode (88.6%), only decayed partially. The contributions of the total decay of ^{121}I and the partial decay of ^{121m}Te were determined and subtracted to deduce the independent cross sections. The obtained cumulative and independent cross sections are presented in Fig. 8. Four earlier publications are available [24,25,26,27] containing only the cumulative experimental cross sections for this reaction. The data of Ismail et al. 1990 [24] and Singh et al. 1997 [27] agree perfectly with our results, while data of Bhardwaj et al. 1994 [26] are somewhat higher below 43 MeV but above this energy their data are lower than our data. The data of Singh et al. 1991 [25] are considerably lower than all the other datasets. As the corresponding publication [25] does not provide enough information about the experiment it is not possible to find the reason for that large deviation.

Table 3
Cross sections for formation of tellurium radioisotopes on ^{nat}Sb target by alpha-particle irradiation.

Energy (MeV)	Cross section (mb)					
	^{nat}Sb(α,x)^{121m}Te cumulative	^{nat}Sb(α,x)^{121m}Te independent	^{nat}Sb(α,x)^{121g}Te cumulative	^{nat}Sb(α,x)^{121g}Te independent	^{nat}Sb(α,x)^{123m}Te	^{nat}Sb(α,x)^{125m}Te
49.93 ± 0.21	65.2 ± 7.7	63.3 ± 9.5	645 ± 73	8.6 ± 2.0	55.2 ± 6.6	32 ± 10
48.94 ± 0.22	54.3 ± 6.5	52.6 ± 8.0	598 ± 68	30.3 ± 6.9	53.9 ± 6.5	40 ± 14
47.92 ± 0.24	39.8 ± 5.0	38.3 ± 6.0	548 ± 62	26.4 ± 6.0	53.4 ± 6.4	23 ± 17
46.87 ± 0.26	37.7 ± 4.8	36.3 ± 5.7	497 ± 56	24.0 ± 5.4	43.6 ± 5.3	11 ± 14
45.81 ± 0.28	25.9 ± 3.6	24.8 ± 4.5	400 ± 45	34.6 ± 7.8	37.1 ± 4.6	20 ± 18
43.92 ± 0.31	16.5 ± 2.3	15.7 ± 3.9	299 ± 34	38.8 ± 8.8	41.0 ± 4.8	54 ± 15
42.78 ± 0.34	10.6 ± 1.4	10.1 ± 2.1	199 ± 23	27.7 ± 6.3	34.0 ± 3.9	27 ± 11
41.61 ± 0.36	8.0 ± 1.2	7.6 ± 1.8	120 ± 14	3.4 ± 0.8	36.8 ± 4.2	44 ± 14
40.40 ± 0.39	3.1 ± 0.7	2.9 ± 1.1	65 ± 7	16.4 ± 3.7	28.5 ± 3.3	55 ± 14
39.17 ± 0.42	1.84 ± 0.9	1.73 ± 0.95	30 ± 3		34.5 ± 4.0	74 ± 17
37.90 ± 0.45	0.08 ± 0.04	0.08 ± 0.05	10.1 ± 1.2	10.0 ± 2.3	28.9 ± 3.3	27 ± 18
35.64 ± 0.51			2.3 ± 0.3	2.3 ± 0.6	30.9 ± 3.5	43 ± 19
34.25 ± 0.55			0.1 ± 0.3	0.1 ± 0.6	35.6 ± 4.1	61 ± 24
31.79 ± 0.62					25.5 ± 2.9	79 ± 33
30.25 ± 0.67					19.4 ± 2.2	197 ± 54
27.51 ± 0.76					13.4 ± 1.6	253 ± 62
25.78 ± 0.82					7.2 ± 0.8	417 ± 78
23.95 ± 0.88					3.7 ± 0.5	343 ± 69
20.58 ± 1.00					0.7 ± 0.2	237 ± 44
16.55 ± 1.13						34 ± 8

An early gamma-measurement, before the complete decay of ^{121}I could be one possible explanation for the published low cross section values. For determining the independent cross sections of the *^{nat}Sb(α,x)^{121g}Te* process contributions from the complete decay of ^{121}I and the partial decay of ^{121m}Te were subtracted from the cumulative cross sections. No earlier data are available for the independent production of ^{121g}Te. The deduced independent cross sections are also included in Fig. 8. The numerical data are collected in Table 3. The prediction of the TALYS model code, taken from the TENDL-2019 database [22], agrees relatively well with the cumulative experimental data, but the calculation for the independent production of ^{121g}Te considerably under estimates the experimental cross sections.

3.3.2. Experimental cross sections of the *^{nat}Sb(α,x)^{123m}Te* process

^{123}Te can be produced on both stable antimony isotopes in the *^{121}Sb(α,np)^{123m}Te* and *^{123}Sb(α,3np)^{123m}Te* reactions, including emission of possible *d* or *t* particles. It is considered as one of the stable isotopes of tellurium with a meta-stable state, ^{123m}Te, ($T_{1/2}$ = 119.2 d). It decays IT (100%) decay mode. Cross sections were determined for formation of the mate-stable state by using its only intense gamma line E_γ = 159.00 keV (I_γ = 84%). The decay of ^{123}I populates only the ground state ^{123}Te, emitting the same E_γ = 159 keV gamma-line. The spectra, measured after long decay time, were used to avoid the contribution of the E_γ = 159 keV gamma-line from decay of ^{123}I to the peak area. No experimental data published earlier were found for this reaction. The newly deduced cross sections are included in Table 3 and in Fig. 9. The shape of the excitation function corresponds to the reactions on the two stable Sb isotopes, having a local maximum at around 34 MeV alpha-particle energy. The TALYS model calculation predicts the shape of the excitation function relatively well, but the amplitude of the curve is somewhat lower than the experimental data.

3.3.3. Experimental cross sections of the *^{nat}Sb(α,x)^{125m}Te* process

The ^{125}Te is one of the stable isotopes of tellurium. The ^{125m}Te ($T_{1/2}$ = 57.4 d) meta-stable state decays with IT decay mode (100%) to the ground state. ^{125m}Te can be formed in the *^{123}Sb(α,d)^{125m}Te* and *^{123}Sb(α,np)^{125m}Te* reactions. Although, reactions only on the ^{123}Sb target isotope contribute to the production of ^{125m}Te the cross sections are presented according to the natural isotopic composition of the target. For data analysis we could use only the E_γ = 35.5 keV (I_γ = 7.3%) gamma line, which is strongly disturbed by decay of ^{125}I ($T_{1/2}$ = 59.400 d). ^{125}I populates only ^{125g}Te. The half-life of ^{125}I is somewhat longer than the half-life of ^{125m}Te. The decays of ^{125}I and ^{125m}Te are independent, but both radionuclides decay to the same daughter, the ^{125g}Te isotope. As mentioned in section 3.2.4. separation of the ^{125}I contribution is possible analytically, by solving the corresponding two unknown-parameters systems of equations based on the spectra collected in the second and third series of the gamma-ray measurements. The separation process resulted in increased uncertainty of the deduced cross sections. Absorption correction for the 35.5 keV gamma-line was calculated for every foil, which included the self-absorption of the Sb layer and the absorption of the covering Kapton layer. The numerical data are collected in Table 3 and are shown in Fig. 10 in comparison with the result of the TALYS model calculation retrieved from the TENDL-2019 database [22]. The model calculation considerably underestimates the experimental cross sections in the whole investigated energy range. No earlier published data were found for this process.

3.4. Production of antimony radionuclides

In principle several antimony isotopes can be produced by a 50 MeV alpha-particle beam on an antimony target. Due to limitations of the applied experimental technique and the used equipments cross sections were possible to determine only for formation of the longer-lived ^{118m}Sb, ^{120m}Sb and ^{122g}Sb radionuclides.

3.4.1. Experimental cross sections of the *^{nat}Sb(α,x)^{118m}Sb* process

The antimony-118 radionuclide has two isomeric states, the shorter-lived ground state ($T_{1/2}$ = 3.6 min) and a longer-lived high spin ($J^\pi = 8^-$) meta-stable state ($T_{1/2}$ = 5.00 h). This radionuclide can be formed in several reactions on the ^{121}Sb target isotope and one additional reaction on the ^{123}Sb target isotope. Due to the short half-life of the ground state it was not assessed. For determining the cross sections for formation of ^{118m}Sb the gamma-spectra collected during the first gamma-measurement series were used. The contribution from decay of ^{118}Te was neglected due to the high reaction threshold energy of E_{th} = 48.26 MeV and the expected low cross section just above the threshold energy of the ^{121}Sb(α,4nt)^{118}Te reaction. The contribution from this reaction, if any, would affect only the highest energy point of our data. The results were obtained based on the two highest intensity gamma-lines as the weighted average of the individual cross sections. The obtained data are presented in Table 4 and in Fig. 11 in comparison with the result of TALYS model calculation [22]. No experimental data were reported for this reaction in the literature earlier. The model calculation basically

Table 4
Cross sections for formation of antimony radioisotopes on ^{nat}Sb target by alpha-particle irradiation.

Energy (MeV)			Cross section (mb)								
			^{nat}Sb(α,x)^{118m}Sb			^{nat}Sb(α,x)^{120m}Sb			^{nat}Sb(α,x)^{122g}Sb cumulative		
49.93	±	0.21	11.5	±	1.4	17.8	±	2.9	39.8	±	4.6
48.94	±	0.22	9.2	±	1.2	17.0	±	2.7	38.3	±	4.4
47.92	±	0.24	5.7	±	0.7	14.4	±	2.3	36.8	±	4.2
46.87	±	0.26	3.5	±	0.6	13.4	±	2.2	35.5	±	4.1
45.81	±	0.28	2.5	±	0.5	12.3	±	2.0	33.3	±	3.9
43.92	±	0.31	0.9	±	0.2	12.4	±	2.0	33.6	±	3.9
42.78	±	0.34	0.2	±	0.2	11.1	±	1.7	29.1	±	3.4
41.61	±	0.36				12.7	±	2.0	31.4	±	3.7
40.40	±	0.39				10.4	±	1.7	23.4	±	2.7
39.17	±	0.42				13.1	±	2.1	27.5	±	3.2
37.90	±	0.45				11.0	±	1.8	21.4	±	2.5
35.64	±	0.51				10.8	±	1.7	19.7	±	2.2
34.25	±	0.55				11.9	±	1.9	19.9	±	2.3
31.79	±	0.62				7.1	±	1.1	11.5	±	1.3
30.25	±	0.67				4.2	±	0.7	6.7	±	0.8
27.51	±	0.76				2.5	±	0.4	4.1	±	0.4
25.78	±	0.82				0.84	±	0.16	1.0	±	0.2
23.95	±	0.88				0.32	±	0.08	0.61	±	0.08
20.58	±	1.00				0.06	±	0.09	0.18	±	0.07
16.55	±	1.13				0.03	±	0.06			

predicts well the excitation function, but with somewhat higher amplitude. The corresponding data were retrieved from the TENDL-2019 data library [22].

3.4.2. Experimental cross sections of the ^{nat}Sb(α,x)^{120m}Sb process

The antimony-120 radionuclide has two isomeric states, the ground state ($T_{1/2}$ = 15.89 min) and a high spin ($J^{\pi} = 8^{-}$) meta-stable state ($T_{1/2}$ = 5.76 d). The level-energy of this meta-stable state is not known. In this experiment the short-lived ground state was not assessed. This radionuclide can be formed in several competing reactions on both of the stable isotopes of the Sb target with the lowest threshold energy of 9.56 MeV. The cross sections for the formation of the meta-stable state were determined as the weighted average, using the three most intense gamma-lines followed the decay of ^{120m}Sb. Spectra measured in the second series were used in the data analysis. The obtained data are included in Table 4 and in Fig. 12 in comparison with the earlier reported experimental data and the result of model calculation. In spite of the relatively low threshold energy the cross sections start to increase only around 20 MeV. The population of this high spin state has lower probability at the lower energy. One experimental dataset was found in the literature [27], which has similar shape as our result but its amplitude is higher by a factor of four. Data reported by the authors for other reactions in the same paper are also too high, which indicates problem in their experiment. The data from the TENDL-2019 database [22] also overestimate our experimental data, however the shape of the excitation function more or less corresponds to the shape of the experimental data.

3.4.3. Experimental cross sections of the ^{nat}Sb(α,x)^{122g}Sb process

The ^{122}Sb radionuclide has two isomeric states, the short-lived ($T_{1/2}$ = 4.191 min) meta-stable state and the longer-lived ($T_{1/2}$ = 2.7238 d) ground state. Cross sections were deduced only for the ground state due to the half-life limitation. As the gamma-ray measurements were started after about one-day cooling time the meta-stable state had decayed completely to the ground state by the IT decay mode. Accordingly, cumulative cross sections were determined for the formation of the ground state. No additional decay contribution was possible. Several reactions with different threshold energies on both stable isotopes of antimony contribute to the formation of ^{122}Sb. The cross sections were determined by using the only intense gamma-line, E_{γ} = 564.24 keV (I_{γ} = 70.68%), which can be considered as an interference-free gamma line. However, ^{123}I emits gamma-photons with an energy within the resolution of the used gamma-detector, but due to its very low intensity (I_{γ} = 0.0011%) its contribution was negligibly small (~0.05%). For the production of ^{122}Sb no decay contribution is possible. The deduced cross sections are included in Table 4 and in Fig. 13. No earlier reported experimental data were found. The TENDL-2019 [22] calculation provides different shape of the excitation function with amplitude in the same range as the experimental data.

4. Summary

Cross sections for alpha-particle induced reactions on natural antimony were measured up to 51 MeV bombarding beam energy. Activation method combined with stacked target technique and gamma-spectrometry measurements were applied. Targets were prepared by vacuum evaporation method using Kapton (polyimide) backing. Measurements were done relative to the ^{nat}Ti(α,x)^{51}Cr monitor reaction. Cross sections for formation of ^{121,123,124,125,126}I, ^{121m,g,123m,125m}Te and ^{118m,120m,122g}Sb were determined and compared to the available literature data and theoretical estimation from the TENDL-2019 data library. Our data improved and in same cases extended to 50 MeV the available data base. Cross sections for formation of ^{121m,123m,125m}Te and ^{118m,122g}Sb were reported for the first time. Comparison of the newly measured experimental cross section data and the predicted values of the TALYS model calculations showed general agreement for most of the investigated processes. However, large deviation was found in case of the ^{nat}Sb(α,x)^{125m}Te reaction, for which considerably smaller predicted values are available in the TENDL-2019 data library.

Declaration of Competing Interest

The authors declare that they have no known competing financial interests or personal relationships that could have appeared to influence the work reported in this paper.

Acknowledgments

This work was performed at the RI Beam Factory operated by RIKEN Nishina Center and CNS, University of Tokyo. This work was partly supported by "Optimization of accelerator production routes of the new theranostic radioisotopes Sc-47 and Cu-67 (JPJSBP120193808 and NKM-43/2019)", under the Japan - Hungary Research Cooperative Program, JSPS and HAS. The work is also supported by JSPS KAKENHI Grant Number 17 K07004.

References:

[1] Thin Film Evaporation Guide, Vacuum Engineering & Materials https://www.vem-co.com/sites/default/files/pdfs/VEM_Thin_Film_Evaporation_Guide_2017.pdf.

[2] A. Hermanne, et al., Reference cross sections for charged-particle monitor reactions, Nucl. Data Sheets 148 (2018) 338–382.

[3] T. Watanabe et al., Beam energy and longitudinal beam profile measurements system at the RIBF, in Proceedings of the 5th International Particle Accelerator Conference (IPAC 2014), 2014, pp. 3566–3568.

[4] H.H. Andersen, J.F. Ziegler, Stopping Powers and Ranges in all Elements, Pergamon, Oxford, 1997.

[5] N.N.D. Center, Nuclear Structure and Decay Data On-Line Library, Nudat 2 (2019) 8. http://www.nndc.bnl.gov/nudat2/.

[6] B. Pritychenko, A. Sonzogni, Q-value Calculator (QCalc), (2003). http://www.nndc.bnl.gov/qcalc/.

[7] International Atomic Energy Agency, LiveChart of Nuclides, (2009). https://www-nds.iaea.org/livechart/.

[8] S. Takács, A. Hermanne, F. Ditrói, F. Tárkányi, M. Aikawa, Reaxamination of cross sections of the ^{100}Mo(p,2n)^{99m}Tc reaction, Nucl. Instrum. Methods Phys. Res. B 347 (2015) 26.

[9] F. Ditrói, S. Takács, H. Haba, Y. Komori, M. Aikawa, Z. Szűcs, M. Saito, Excitation function of the alpha particle induced nuclear reactions on enriched ^{116}Cd, production of the theranostic isotope ^{117m}Sn, Nucl. Instrum. Methods Phys. Res. B 385 (2016) 1124.

[10] S. Takács, F. Ditrói, Z. Szűcs, H. Haba, Y. Komori, M. Aikawa, M. Saito, Crosschecking of alpha particle monitor reactions up to 50 MeV, Nucl. Instrum. Methods Phys. Res. B 397 (2017) 33–38.

[11] S. Takács, M.P. Takács, F. Ditrói, M. Aikawa, H. Haba, Y. Komori, Activation cross sections of longer-lived radionuclides produced in germanium by alpha particle irradiation, Nucl. Instrum. Methods Phys. Res. B 383 (2016) 213.

[12] F. Ditrói, S. Takács, H. Haba, Y. Komori, M. Aikawa, Cross section measurement of alpha particle induced nuclear reactions on natural cadmium up to 52 MeV, Appl. Radiat. Isot. 118 (2016) 266.

[13] S. Takács, F. Ditrói, Z. Szűcs, M. Aikawa, H. Haba, Y. Komori, M. Saito, Measurement of activation cross sections of alpha particle induced reactions on iridium up to an energy of 50 MeV, Appl. Radiat. Isot. 136 (2018) 133–142.

[14] F. Ditrói, S. Takács, H. Haba, Y. Komori, M. Aikawa, M. Saito, T. Murata, Investigation of alpha particle induced reactions on natural silver in the 40–50 MeV energy range, Nucl. Instrum. Methods Phys. Res. B 436 (2018) 119–129.

[15] M. Aikawa, M. Saito, Y. Komori, H. Haba, S. Takács, F. Ditrói, Z. Szűcs, Activation cross sections of alpha-particle induced nuclear reactions on natural palladium, Nucl. Instrum. Methods Phys. Res. B 449 (2019) 99–104.

[16] M. Saito, M. Aikawa, T. Murata, N. Ukon, Y. Komori, H. Haba, S. Takács, Activation cross sections of alpha-induced reactions on natural ytterbium up to 50, Nucl. Instrum. Methods Phys. Res. B 453 (2019) 15–21.

[17] T. Murata, M. Aikawa, M. Saito, H. Haba, Y. Komori, N. Ukon, S. Takács, F. Ditrói, Excitation function measurement for zirconium-89 and niobium-90 production using alpha-induced reactions on yttrium-89, Nucl. Inst. Methods Phys. Res. B 458 (2019) 21-27.

[18] Sándor Takács, Masayuki Aikawa, Moemi Saito, Tomohiro Murata, Naoyuki Ukon, Yukiko Komori, Hiromitsu Haba, Activation cross sections of alpha particle-induced reactions on natural hafnium up to 50 MeV, Nucl. Inst. Methods Phys. Res. B 459 (2019) 50–58.

[19] Moemi Saito, Masayuki Aikawa, Tomohiro Murata, Yukiko Komori, Hiromitsu Haba, Sándor Takács, Ferenc Ditrói, Zoltán Szűcs, Production cross sections of 169Yb by the proton-induced reaction on 169Tm, Nuclear Inst. and Methods in Physics Research B 471 (2020) 13–16.

[20] S. Takács, M. Aikawa, H. Haba, Y. Komori, F. Ditrói, Z. Szűcs, M. Saito, T. Murata, M. Sakaguchi, N. Ukon, Cross sections of alpha-particle induced reactions on ^{nat}Ni: Production of ^{67}Cu, Nucl. Inst. Methods Phys. Res. B 479 (2020) 125–136.

[21] G. Deconninck, Introduction to radioanalytical physics, Nuclear Methods Monograph series, Akadémia Kiadó, Budapest, 1978, pp. 64 - 72.

[22] A.J. Koning et al., Nucl. Data Sheets 155, (2019) 1, TENDL-2019: Database available from:URL: https://tendl.web.psi.ch/tendl_2019/tendl2019.html.

[23] N. Otuka, E. Dupont, V. Semkova, B. Pritychenko, A.I. Blokhin, M. Aikawa, S. Babykina, M. Bossant, G. Chen, S. Dunaeva, R.A. Forrest, T. Fukahori, N. Furutachi, S. Ganesan, Z. Ge, O.O. Gritzay, M. Herman, S. Hlavač, K. Katō, B. Lalremruata, Y.O. Lee, A. Makinaga, K. Matsumoto, M. Mikhaylyukova, G. Pikulina, V.G. Pronyaev, A. Saxena, O. Schwerer, S.P. Simakov, N. Soppera, R. Suzuki, S. Takács, X. Tao, S. Taova, F. Tárkányi, V.V. Varlamov, J. Wang, S. C. Yang, V. Zerkin, Y. Zhuang, Towards a More Complete and Accurate Experimental Nuclear Reaction Data Library (EXFOR): International Collaboration Between Nuclear Reaction Data Centres (NRDC), Nucl. Data Sheets 120 (2014) 272–276.

[24] M. Ismail, Measurement and analysis of the excitation function for alpha-induced reactions on Ga and Sb isotopes, Phys. Rev. C 41 (1990) 87.

[25] B.P. Singh, H.D. Bhardwaj, R. Prasad, A study of pre-equilibrium emission in alpha-induced reactions on ^{121,123}Sb, Can. J. Phys. 69 (1991) 1376.

[26] M.K. BHARDWAJ, I.A. RIZVI, A.K. CHAUBEY, Alpha-induced reactions in antimony, Int. J. Modern Phys., Part E 03 (01) (1994) 239–248.

[27] N.L. Singh, D.J. Shan, S. Mukherjee, S.N. Chintalapudi, Excitation functions for alpha-particle induced reactions with natural antimony, Nuovo Cimento A 110 (1997) 693.

[28] I.A. Watson, S.L. Waters, D.J. Silvester, Excitation functions for the reactions producing 121-I, 123-I and 124-I from irradiation on natural antimony with 3-He and 4-He particles with energies up to 30 MeV, J. Inorg. Nucl. Chem. 35 (1973) 3047.

[29] Y. Homma, Y. Murakami, Production of ^{123}I by bombarding a antimony target with alpha and 3He particles, Radioisotopes 25 (1976) 314.

[30] A. Calboreanu, C. Pencea, O. Salagean, The effect of gamma de-excitation competition on the (α, n) and (α,2n) reactions on gold and antimony, Nucl. Phys. A 383 (1982) 251.

[31] K.F. Hassan, S.M. Qaim, Z.A. Saleh, H.H. Coenen, Alpha particle induced reactions on ^{nat}Sb and ^{121}Sb with particular reference to the production of the medically interesting radionuclide ^{124}I, Appl. Radiat., Isot. 64 (2006) 101.

[32] F. Tárkányi, S. Takács, B.Király, F. Szelecsényi, L. Andó, J. Bergman, S-J. Heselius, O. Solin, A. Hermanne, Yu.N. Shubin, A.V. Ignatyuk, Excitation functions of 3He- and α- particle induced nuclear reactions on natSb for production of medically relevant 123I and 124I radioisotopes, Appl., Radiat., Isot. 67 (2009) 1001.

[33] M.S. Uddin, A. Hermanne, S. Sudár, M.N. Aslam, B. Scholten, H.H. Coenen, S. M. Qaim, Excitation functions of alpha-particle induced reactions on enriched Sb-123 and Sb-nat for production of I-124, Appl., Radiat., Isot. 69 (2011) 699.

[34] B.P. Singh, M.K. Sharma, M.M. Musthafa, H.D. Bhardwaj, R. Prasad, A study of pre-quilibrium emission in some proton- and alpha-induced reactions, Nucl. Intr. Method A 562 (2006) 717.

[35] Z. Korkulu, N. Ozkan, G.G Kiss, T. Szucs, Gy. Gyurky, Zs. Fulop, R.T. Guray, Z. Halasz, T. Rauscher, E. Somorjai, Zs. Torok, C. Yalcin), Investigation of alpha-induced reactions on Sb isotopes relevant to the astrophysical gamma-process, Phys. Rev. C 97 (2018) 045803.

[36] Photon Interaction Database, National Institute of Standards and Technology, (2004). https://physics.nist.gov/PhysRefData/XrayMassCoef/tab3.html.

[37] P.F. Mantica Jr., B.E. Zimmerman, W.B. Walters, D. Rupnik, E.F. Zganjar, J. Kormicki, H.K. Carter, W.-D. Schmitt-Ott, Level structures of ^{119}Te and ^{121}Te populated in the decay of ^{119}I and ^{121}I, Phys. Rev. C 42 (1990) 1312.